

Detecting Multiple Cysts in the Kidney with the Development of an Active Contour Method Based on Kidney Ultrasound (USG) Images

¹Mardison, ²Yuhandri, ³Muhammad Tajuddin

Submitted: 28/04/2023

Revised: 28/06/2023

Accepted: 08/07/2023

Abstract: This study examined digital 2-Dimensional (2D) Ultrasonography (USG) images of human kidneys. The ultrasound image was captured with an ultrasound instrument that locates items in the human body by employing sound pressure waves that fluctuate at a very high frequency (ultrasonic). This study aimed to improve kidney 2D ultrasound imaging using the Active Contour approach to find many kidney cysts. The technique used in this study is marker detection, referred to as process 1, followed by a contour initialization step, as process 2, before mapping the area of kidney cysts using the active contour method and the binary segmentation method, as process 3. The identification of renal cysts leads to the subsequent phase of RGB segmentation. The results of 43 2D ultrasound scans of the kidney from this study yielded an accuracy rate of 88.37%, with 38 images correctly identifying kidney cysts and five images incorrectly identifying kidney cysts.

Keywords: *Ultrasonography Image, USG, Multiple Kidney Cysts, Active Contour Method.*

1. Introduction

An ultrasound image, also called ultrasound, can be used to take pictures of objects inside the human body [1]–[4]. Using ultrasound pictures in healthcare and medicine is widespread to ascertain the state of the human organs when the image was taken [5]–[8]. There are three categories of ultrasound images: 2D, 3D, and 4D. 2D ultrasound examines where the imaging outcomes form flat, monochrome images. The kidney is one of the many human organs seen in ultrasound pictures.

The kidneys are a pair of human organs situated on either side of the human spine, below the rear of the ribs, and close to the center of the back. One of the organs crucial in maintaining human life is the kidney [9]–[11]. The fact that the kidney comprises two parts—the left kidney and the right kidney—indicates that it is an organ developed in pairs. The average kidney is between 10 and 12 cm in size, or about the size of a human fist [12]–[14]. Roughly one million nephrons, microscopic blood filters, are present in this organ. This relatively small organ has some significant tasks in maintaining bodily health. Every day, the kidneys filter around 200 liters of blood.

Simple definition: Kidney cysts are fluid-filled sacs that develop inside or on the surface of the kidneys [15]–[18]. There are four different forms of kidney cysts, with noncancerous or simple kidney cysts being the most prevalent. Simple kidney cysts rarely result in renal problems or failure [19]–[21]. Age and gender are risk variables that increase a person's vulnerability to kidney cysts. Kidney cyst disease is more likely to affect older people. Simple kidney cysts typically do not have distinct symptoms or indicators. Symptoms will show when the cyst gets big enough or puts pressure on other organs.

Only 2D black-and-white images, which are still hazy or blurry, are currently produced by ultrasonic technology, specifically the kidney of a human being captured by ultrasound [22]–[24]. As a result, a professional urologist will misread renal ultrasound results. The caliber of the ultrasound image generated determines the accuracy of the urologist's reading or translation of the ultrasound image [25]–[28]. To ensure an accurate and precise diagnosis of a person's ailment, the readings or translations done by a urologist must also be accurate and precise. In these circumstances, the USG image should be enhanced to be crisper and more detailed to increase the precision and accuracy of the reading findings.

According to conversations he had with a professional urologist in Padang, the images created by 2D ultrasound are still fuzzy, making it impossible for an expert urologist to detect cystic items in human kidney organs at this time and less distinct. The human kidney can be imaged with a CT (Computed Tomography) Scan for more precisely detecting kidney cysts. However, a CT Scan is quite expensive, and not all Indonesian hospitals (RS) have a CT Scanner because of the high cost of such

¹ Information System, Universitas Putra Indonesia YPTK Padang, Lubuk Begalung Highway, Padang, 25221, Indonesia. Email ID: mardison@upiypk.ac.id

² Information Technology, Universitas Putra Indonesia YPTK Padang, Lubuk Begalung Highway, Padang, 25221, Indonesia. Email ID: yuyu@upiypk.ac.id

³ Information Technology, Universitas Putra Indonesia YPTK Padang, Lubuk Begalung Highway, Padang, 25221, Indonesia. Email ID: tajuddin@universitasbumigora.ac.id

a scanner.

Specifically, according to a search of renowned international publications and impact factors, researchers have yet to attempt to identify Multiple Kidney cysts or what is known as Multiple Kidney cysts. Suppose a 2D kidney ultrasound image cannot produce results as accurate and digital as a human kidney CT (Computed Tomography) Scan in identifying multiple kidney cysts. In that case, it will benefit hospitals offering treatment and the medical community. It applies especially to the area of urology, particularly when it comes to kidney issues. It can provide significant advantages for those suffering from kidney disease. Based on 2D ultrasound (ultrasonography) images of human kidneys, this study introduces the Active Contour approach to detect automatically numerous kidney cysts. The outcomes of this investigation were validated using CT-Scan image data of the human kidney that a urologist approved.

2. Related work

Khurram Ejaz et al.'s [29] earlier research found confidence areas and contour detection on MRI images. This study aims to create an area of interest (ROI) technique for brain tumor MRI images by identifying intensity fluctuations using a confidence score. For complex cases of tumor core extension, this study suggests a contour detection approach with confidence region (CRCR) to highlight the borders of tumor tissue. The study finds that the tumor area may be extracted using the CRCR approach. The average results are DOI 0.97, JI 0.94, MSE 1.24 dB, and a peak signal-to-noise ratio of 17.45 dB.

Saleem Mustafa et al. [30] segmented Saleem's skin lesions in a different study using the Adaptive Active Contour approach based on entropy and Gaussian filters. This study uses maximum entropy and morphological processing techniques based on Gaussian filters to determine the automatic beginning points for active contours. According to the findings, the procedure is superior to dermatologists' segmented images. He thus focuses on mask selection for active contours and morphological procedures such as preprocessing and postprocessing for active contours.

In another investigation, Frank G. Zöllner et al. [31] performed kidney segmentation in magnetic resonance imaging of the kidney's present status and outlook. This article evaluates recent research on renal image segmentation methods and highlights the shortcomings of recently presented methods that might impede clinical application. Following range thresholding, several binary morphological processes remove regions representing vessels and collecting systems. Based on a variation framework, the Resilient Statistical Segmenter (RSS) software was run in 3D Slicer to drive the development of closed surfaces by minimizing energy functions. The approaches need to be compared and assessed in greater

detail. Consequently, it is necessary for the publicly accessible data set to be correct.

3. Methodology

3.1 Research Framework

This research aims to improve Ultrasound images of the kidneys by developing the Active Contour method, which can be used to detect multiple kidney cysts, to provide unlimited access for Urologists, and to diagnose multiple kidney cysts. Figure 1. Stages of this Research:

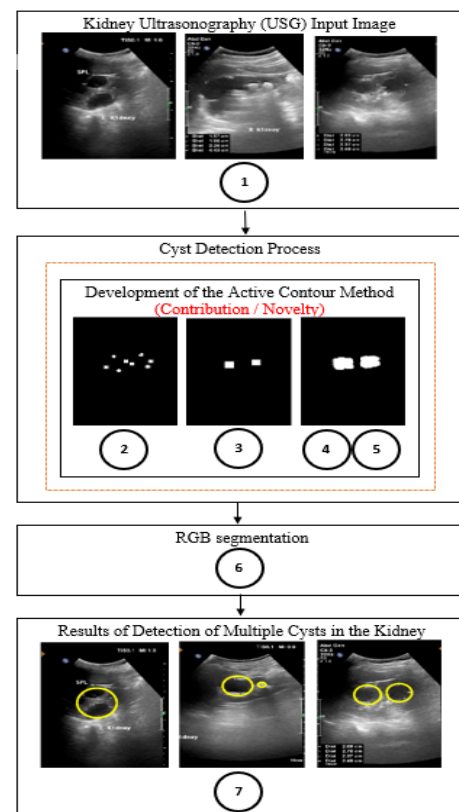


Fig. 1. Research Framework

3.2 Research Framework Details

3.2.1 Kidney Ultrasonography (USG) Input Image

Ultrasonography (USG) image input contains original image data used as input data in research. The image data used as input is USG imagery in a digital file with *.jpg format. All test images used are grayscale images with a pixel size of 1080 x 1350 pixels, where the purpose of this site is for the process of dimensional uniformity of the test images to be studied. The test images consist of 43 ultrasound images of human kidneys with multiple kidney cysts. As sample images in this study, we present three images. Figure 2 below shows an example of a 2D Ultrasound image of the Human Kidney.

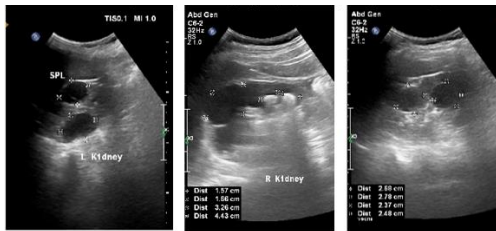


Fig 2. Research Framework

3.2.2 Cyst Area Detection (Process 1)

The ultrasound image of the kidney is inputted into the system then the researcher performs the detection stage of the cyst area in the image. An outline of possible markers is found to detect the object desired while excluding other objects that do not require detection. Next concludes the location of the corner markers in the image. In addition, a cyst area detection system is used to confirm that it is a marker and decipher its identity. The system also uses cyst area detection to calculate the pose using the information from the location of the detected marker. Below is Algorithm 1, which the researcher uses to detect image areas of the cyst area detection process.

Algorithm 1: Cyst Area Detection (Process 1)

1. Reading digital ultrasound images of multiple kidney cysts
 2. Detecting cyst area 1 and named A
 3. Detecting cyst area 2 and named B
 4. Detecting cyst area 3 and named C
 5. Calculating the centroid and circularity area values for cysts A, B, and C
 6. Displaying the image of the detection of the cyst area
-

3.2.3 Contour Initialitation (Process 2)

Contour initialization recognizes the coordinate positions of all Cyst Areas detected in the image to become a single object or a particular pattern to be recognized as a complete object [32], [33]. In this study, the ultrasound image of the kidney, which had been detected by the cyst area in the previous step, distinguished the boundaries of cysts on the kidneys from those not cysts on the kidneys. Below is Algorithm 2 used to initialize the image contour.

Algorithm 2: Contour Initialization

1. Reading the image of the cyst area detection results
 2. Recognizing the coordinates of the cyst area in the image
 3. Activating the cyst area coordinates as object boundaries
 4. Saving the cyst area coordinate values as object
-

boundaries

5. Connecting each cyst area coordinate as an object boundary line
 6. Saving the object outline as a contour
 7. Displaying the outline of the object
 8. Calculating the centroid and circularity area values for cysts A, B, and C
 9. Displaying the image of the detection of the cyst area
-

3.2.4 Robert Edge Detection

Robert Edge Detection is the ability to reduce noise in the image before performing edge detection calculations [34]–[36]. The objective is to ensure that edge detection is carried out precisely and accurately. Each detection method has many sub-methods, but a suitable image detection method can eliminate as much noise as possible. Below is Algorithm 3 that researchers use to perform Robert Edge Detection.

Algorithm 3: Robert Edge Detection

1. Reading the initialized contour image
 2. Reading the values of the contour initialization matrix
 3. Taking a value that means a gray image in the form I_x and I_y
 4. Calculating the edge values of objects in the image with the formula: $\sqrt{I_x^2 + I_y^2}$
 5. Storing the edge value of the object in the image
 6. Displaying object edges in the image
-

3.2.5 Cyst Area Mapping: The Proposed Algorithm from Active Contour Method (Process 3) / Biner Segmentation

Active contour is a segmentation method using a closed curve model that can move wide or narrow [37]–[39]. Active contour can move widened or narrowed by minimizing image energy using external force and is influenced by image characteristics such as lines or edges. This study uses Active Contour to strengthen the boundaries or edges of image objects detected by the Robert Edge Detection method to ensure that the objects detected are more precise and accurate. Below is Algorithm 4, developed to become a new algorithm based on the active contour method. This research proposes an algorithm, Process 3, to map the cyst area of the kidney. The result of this process is namely Biner Segmentation.

Algorithm 4: The Proposed Algorithm from Active Contour Method (Process 3)

1. Reading the image of Robert's Edge Detection
2. Activating the edge of the image as a contour
3. Saving the contour activation value
4. Reading the image of the active contour results
5. Performing opening morphological operations
6. Saving the image of the results of the opening morphology operation
7. Reading the resulting binary segmentation image (active contour)
8. Saving the resulting binary segmentation image
9. Displaying the result of binary segmentation image

3.2.6 Opening Morphology (RGB Segmentation)

Image morphology operation is a process that aims to change the shape of objects in the original image [40], [41]. This process can be done on grayscale images or binary images. The morphological surgery research carried out is opening morphology surgery. The morphology of the opening involves an erosion operation followed by dilation of the outer surface of the foreground in the image. This operation combines two main methods, usually used to remove noise from images. This opening morphology process is carried out to change images that have successfully detected the edges of grayscale-shaped objects into binary to make the image detection cleaner. Below is Algorithm 5, which researchers use to perform opening morphology.

Algorithm 5: Opening Morphology (RGB Segmentation)

1. Reading the image of the active contour results
2. Performing opening morphological operations
3. Saving the image of the results of the opening morphology operation
4. Reading the RGB segmentation image (opening morphology)
5. Saving the RGB segmentation image
6. Displaying the RGB segmentation result image

3.2.7 Kidney Cyst Detection Result

The results of detecting kidney cysts are the final process in this study displaying which part of the ultrasound image of the kidney is a kidney cyst. The detection results in the final result and accumulation of the previous process.

3.2.8 GUI Design of Kidney Ultrasound Multiple Cyst Detection Application

GUI Design of Multiple Kidney Ultrasound Cyst Detection Applications can be seen in Figure 3 below:

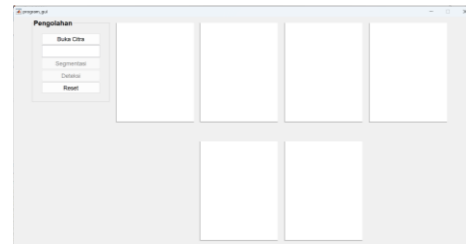


Fig. 2. Design of Multiple Kidney Ultrasound Cyst Detection Application

4. Result and Discussion

This research was conducted through several stages. The first stage is Data Collection. Its first step is collecting three ultrasound images of the human kidneys. After the data are collected, it continues in the second stage, called the Preprocessing stage, including detecting the cyst area, initializing the contour, and detecting the edge of Robert. Furthermore, the processing is carried out in an active contour process and closing morphological operation. The processing section, which is a novelty or updated in this study, is the Active Contour method. Next is the result section, displaying the Binary Image Segmentation Results, RGB Image Segmentation Results, and Multiple Kidney Cyst Image Detection Results.

4.1 Kidney Ultrasonography (USG) Input Image

The test images consist of 25 soil images. All soil images collected are images of land used as agricultural land for food crops in the Solok Regency, West Sumatra province. All soil images collected were from six types of plants grown on the soil, namely Red Chilli, Green Chilli, Red Onions, Peanuts, Potatoes, and Cabbages. As sample images in this study, we present 5 images. In table 1 below you can see an example of a soil image.

Table 1. Input Image Result

No	USG Image	Name
1		Kidney Ultrasound Image of Patient 1 (Multiple Kidney Cyst 1)
2		Kidney Ultrasound Image of Patient 2 (Multiple Kidney Cyst 2)

3		Kidney Ultrasound Image of Patient 3 (Multiple Kidney Cyst 3)
---	---	---

4.2 Cyst Area Detection (Process 1)

Table 1 above shows the ultrasound images of the kidneys from three patients with multiple kidney cysts in their kidneys. Number 1 is the ultrasound image of the multiple kidneys of Patient 1, Number 2 is the ultrasound image for Patient 2, and Number 3 is for Patient 3. In this image, the doctor specializing in urology marks which part of the image boundaries includes kidney cysts and which does not.

Table 2. Cyst Area Detection (Process 1) Result

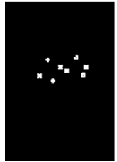
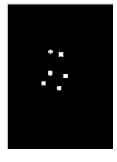
No	USG Image	Cyst Area Detection Image (Process 1)	Name
1			Kidney Ultrasound Image of Patient 1 (Multiple Kidney Cyst 1)
2			Kidney Ultrasound Image of Patient 2 (Multiple Kidney Cyst 2)
3			Kidney Ultrasound Image of Patient 3 (Multiple Kidney Cyst 3)

Table 2 above shows the results of detecting cyst areas on ultrasound images of kidneys with multiple kidney cysts. In the image of the cyst area detection results, white dots indicate that a cyst area is well detected on an ultrasound image of the kidney. In the image of a patient with multiple kidney cysts 1, it can be seen that eight white dots grouped in as many as two groups forming a group of images like circles side by side corresponding to the cyst area made by the doctor. In the image of a patient with multiple kidney cysts 2, there are six white dots in groups

of two groups forming a circle-like image group side by side corresponding to the cyst area made by the doctor. The image of a patient with multiple kidney cysts 3 shows that six white dots are grouped in as many as two groups forming a circle-like image group close together, one large and the other small corresponding to the cyst area made by the doctor.

4.3 Initialization Contour (Process 2)

Table 3. Initialization Contour (Process 2) Result

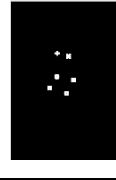
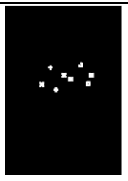
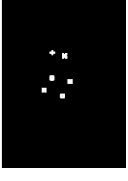
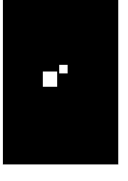
No	USG Image	Cyst Area Detection Image (Process 1)	Initialization Contour (Process 2)
1			
2			
3			

Table 3 shows the results of the initialization of the contour on the ultrasound image of the kidney, which has multiple kidney cysts. In the image from the initialization of the contour, it can be seen that the white dots are fewer in number but with a larger size. It indicates that the area around it is the area of multiple kidney cysts. In image number 1, two white dots are the same size as a box or square shape side by side, whose position corresponds to the previously detected Cyst Area. Image number 2 also has two white dots that are not the same size, one is large, and the other is small, like a box or square shape side by side, whose position corresponds to the Cyst Area previously detected. Two white dots are not the same size in image number 3, one is large, and the other is small, like a box or square shape side by side, whose position corresponds to the Cyst Area previously detected.

4.4 Robert Edge Detection and Cyst Area Mapping: The Proposed Algorithm from Active Contour Method (Process 3) / Biner Segmentation

Table 4. Robert Edge Detection And Cyst Area Mapping: The Proposed Algorithm From Active Contour Method (Process 3) / Biner Segmentation

No	USG Image	Process 1	Process 2	Process 3
1				
2				

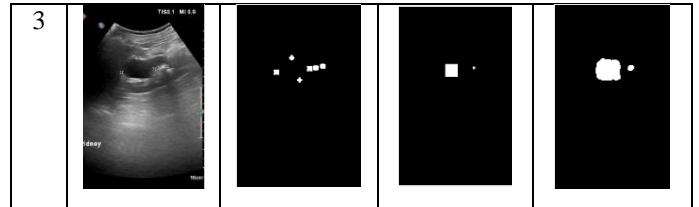
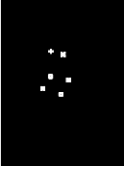
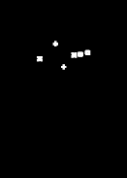
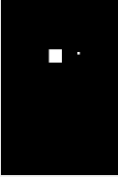


Table 4 above shows the results of binary segmentation on ultrasound images of kidneys with multiple kidney cysts. In the binary segmentation result image, it can be seen that two irregularly shaped areas are white, and outside the region are black. It indicates that the white areas are kidney cysts, and the black ones are not. The white area corresponds to the cyst area that the specialist urologist removed. Image number 1 shows two white areas, one large and the other slightly smaller, and the two areas are separated. In image number 2, it can be seen that the two areas are united or not separated. In image number 3, there are two white areas; one is large, the other is much bigger, and the two separate areas.

4.5 Opening Morphology (RGB Segmentation)

Table 5. Opening Morphology (RGB Segmentation) Result

No	USG Image	Process 1	Process 2	Process 3	RGB Segmentation Results
1					
2					
3					

In Table 5, it can be seen the results of binary segmentation on ultrasound images of kidneys with multiple kidney cysts. In the binary segmentation result image, it can be seen that two irregularly shaped areas are white, and outside the region are black. It indicates that the white areas are kidney cysts, and the black ones are not. The white area corresponds to the cyst area made by a specialist urologist. In image number 1, there are two white areas, one large and

the other slightly smaller, and the two areas are separated. In image number 2, it can be seen that the two areas are united or not separated. Image number 3 shows two white areas; one is large, the other is much bigger, and the two areas are separated.

4.6 Kidney Cyst Detection Result

Table 6. Kidney Cyst Detection Result

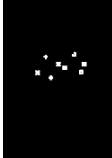
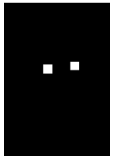
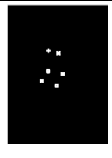
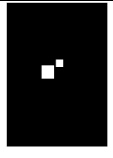
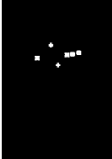
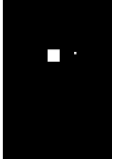
No	USG Image	Cyst Area Detection (Process 1)	Contour Initialization (Process 2)	Cyst Area Mapping (Process 3)	RGB Segmentation Results	Kidney Cyst Detection Result
1						
2						
3						

Table 6 above shows the results of binary segmentation on ultrasound images of kidneys with multiple kidney cysts. In the binary segmentation result image, it can be seen that two irregularly shaped areas are white, and outside the region are black. It indicates that the white areas are kidney cysts, and the black ones are not. The white area corresponds to the cyst area that a specialist urologist removes. In image number 1, it can be seen that there are two white areas, one large and the other slightly smaller, and the two areas are separated. In image number 2, two areas are united or not separated. In image number 3, there are two white areas; one is large, the other is much bigger, and the two areas are separated.

4.7 Comparison of Results with the Old Active Contour Method and the New Active Contour Method

The old Active Contour method could only detect the subtle boundaries of the area between kidney cysts and those that were not. The only limitation that can be made with the old Active Contour method is in the form of jagged images that need to be more precise or better that the detection results are imprecise and inaccurate. The following is Table 4.8. comparing the results of the detection of multiple kidney cysts with the old method and the results of the detection of multiple kidney cysts with the new method developed in this study.

Table 7. Comparison of results with the old active contour method and the new active contour method

No	USG Image	Old Active Contour Method	New Active Contour Method	Process 3
1				The image of the Detection Results of the Old Active Contour Method cannot mark the area of a kidney cyst, while the new Active Contour method can mark it with a yellow circle shape.
2				The image of the Detection Results of the Old Active Contour Method cannot mark the area of a kidney cyst, while the new Active Contour method can mark it with a yellow circle shape.

3				<p>The image of the Detection Results of the Old Active Contour Method cannot mark the area of a kidney cyst, while the new Active Contour method can mark it with a yellow circle shape.</p>
---	---	---	---	---

4.8 Comparison of the Formulas of the Old Active Contour Method with the New Active Contour Method

The Active Contour method has a formula for running the contour activation process properly and correctly. In this study, the formula was modified to make the detection process of multiple kidney cysts more precise and accurate. The following Table VIII shows a comparison of the formula for the old active contour method with the new one:

Old Active Contour Formula
$E_{snake} = \int_{s=0}^1 E_{int}(v(s) + E_{img} + E_{con}v(s))ds$ <p>Information:</p> <ul style="list-style-type: none"> - E_{snake} = Is an energy function of the active contour; from this function, an object that fulfills this energy function will be sought. - $v(s)$ = Is a collection of x and y coordinates of the active contour curve. - E_{int} = Is the internal energy of the active contour. This energy affects the movement of the active contour curve. - E_{img} = Is the energy of the digital image as input (low-level features such as edge points). - E_{con} high-level information that affects the movement of the active contour curve.
New Active Contour Formula
$\min_dist = \min(\text{centroid})$ $\max_dist = \max(\text{centroid})$ $d = \sqrt{(\min_dist(1) - \max_dist(1))^2 + (\min_dist(2) - \max_dist(2))^2}$ $d = \frac{d}{6}$ <p>Information:</p> <ul style="list-style-type: none"> - \min_dist = The closest (minimum) distance to the centroid (object center point) - \max_dist = The farthest (maximum) distance to the centroid (object center point) - d = Object Diameter

5 Conclusion

Based on the analysis and discussion results, conclusions are drawn regarding the achievement of the objectives, namely: An Active Contour method has been developed called Active Contour MD, which can detect multiple kidney cysts properly, precisely, and accurately from 2D ultrasound images of the kidneys. The development of the Active Contour method obtained an accuracy rate of 88.37% from the results of 43 2D ultrasound images of the kidney and found that 38 images correctly detected kidney cysts and five images that were not quite right for detecting kidney cysts. This development method can not only be used to detect multiple kidney cysts but also can be used to detect single kidney cysts.

Acknowledgment

We would like to thank the Yayasan Perguruan Tinggi Komputer (YPTK) Padang, especially the chairman of the Foundation, Mrs. Dr. Hj. Zerni Melmusi, M.M., Ak. CA. and the Advisory Chairman of YPTK Padang, Mr. Dr. Muhammad Ridwan, S.E., M.M., who have supported and funded all of this research, and Universitas Putra Indonesia YPTK Padang, which has facilitated and guided this research.

References

- [1] L. Fang and X. Wang, "Ultrasound COVID-19 classification based on the novel module-based dual-path Network," *IEEE Trans. Artif. Intell.*, vol. PP, pp. 1–12, 2022, doi: 10.1109/TAL.2022.3208217.
- [2] Y. Lu, K. Li, B. Pu, Y. Tan, and N. Zhu, "A YOLOX-based Deep Instance Segmentation Neural Network for Cardiac Anatomical Structures in Fetal Ultrasound Images," *IEEE/ACM Trans. Comput. Biol. Bioinforma.*, vol. PP, no. Xx, pp. 1–12, 2022, doi: 10.1109/TCBB.2022.3222356.
- [3] X. Liu *et al.*, "Scale Mutualized Perception for Vessel Border Detection in Intravascular Ultrasound Images," *IEEE/ACM Trans. Comput. Biol. Bioinforma.*, pp. 1–12, 2022, doi: 10.1109/TCBB.2022.3224934.
- [4] L. Zhao, N. Li, G. Tan, J. Chen, S. Li, and M. Duan, "The End-to-end Fetal Head Circumference Detection and Estimation in Ultrasound Images," *IEEE/ACM Trans. Comput. Biol. Bioinforma.*, vol. 99, no. 1, pp. 1–13, 2022, doi: 10.1109/TCBB.2022.3227037.
- [5] B. L. West *et al.*, "Tetris: Using Software/Hardware Co-Design to Enable Handheld, Physics-Limited 3D Plane-Wave Ultrasound Imaging," *IEEE Trans. Comput.*, vol. 69, no. 8, pp. 1209–1220, 2020, doi: 10.1109/TC.2020.2990061.

- [6] D. Sheng, J. W. Lin, Y. H. Wang, and C. C. Huang, "High-Resolution All-Digital Transmit Beamformer for High-Frequency and Wearable Ultrasound Imaging Systems," *IEEE Trans. Very Large Scale Integr. Syst.*, vol. 28, no. 2, pp. 492–502, 2020, doi: 10.1109/TVLSI.2019.2950707. S. Baluja, "Hiding Images within Images," *IEEE Trans. Pattern Anal. Mach. Intell.*, vol. 42, no. 7, pp. 1685–1697, 2020, doi: 10.1109/TPAMI.2019.2901877.
- [7] F. Lin *et al.*, "Mobile Communication Among COTS IoT Devices via a Resonant Gyroscope With Ultrasound," *IEEE/ACM Trans. Netw.*, vol. 31, no. 3, pp. 1026–1041, 2022, doi: 10.1109/TNET.2022.3205151.
- [8] A. Piana *et al.*, "Small renal masses in kidney transplantation: Overview of clinical impact and management in donors and recipients," *Asian J. Urol.*, vol. 9, no. 3, pp. 208–214, 2022, doi: 10.1016/j.ajur.2022.06.001.
- [9] R. G. Langham *et al.*, "Kidney health for all: Bridging the gap in kidney health education and literacy," *Nefrologia*, vol. 42, no. 2, pp. 113–121, 2022, doi: 10.1016/j.nefro.2022.05.001.
- [10] D. Winitzki *et al.*, "Educational Attainment Is Associated With Kidney and Cardiovascular Outcomes in the German CKD (GCKD) Cohort," *Kidney Int. Reports*, vol. 7, no. 5, pp. 1004–1015, 2022, doi: 10.1016/j.ekir.2022.02.001.
- [11] R. Murugan, M. Y. Boudreaux-Kelly, J. A. Kellum, P. M. Palevsky, and S. Weisbord, "Kidney Cell Cycle Arrest and Cardiac Biomarkers and Acute Kidney Injury Following Angiography: The Prevention of Serious Adverse Events Following Angiography (PRESERVE) Study," *Kidney Med.*, vol. 5, no. 3, p. 100592, 2023, doi: 10.1016/j.xkme.2022.100592.
- [12] M. Hassanein *et al.*, "Dysnatremias, Mortality, and Kidney Failure in CKD: Findings From the Chronic Renal Insufficiency Cohort (CRIC) Study," *Kidney Med.*, vol. 4, no. 12, p. 100554, 2022, doi: 10.1016/j.xkme.2022.100554.
- [13] T. Browne *et al.*, "Improving Access to Kidney Transplantation: Perspectives From Dialysis and Transplant Staff in the Southeastern United States," *Kidney Med.*, vol. 3, no. 5, pp. 799–807.e1, 2021, doi: 10.1016/j.xkme.2021.04.017.
- [14] D. Szaraz *et al.*, "Primary cilia and hypoxia-associated signaling in developmental odontogenic cysts in relation to autosomal dominant polycystic kidney disease – A novel insight," *HELIVON*, p. e17130, 2023, doi: 10.1016/j.heliyon.2023.e17130.
- [15] C. Hanna *et al.*, "Kidney Cysts in Hypophosphatemic Rickets With Hypercalciuria: A Case Series," *Kidney Med.*, vol. 4, no. 3, p. 100419, 2022, doi: 10.1016/j.xkme.2022.100419.
- [16] A. V. Gregory *et al.*, "Utility of new image-derived biomarkers for autosomal dominant polycystic kidney disease prognosis using automated instance cyst segmentation," *Kidney Int.*, pp. 1–9, 2023, doi: 10.1016/j.kint.2023.01.010.
- [17] S. Barone *et al.*, "Identification of an Electrogenic 2Cl⁻/H⁺ Exchanger, ClC5, as a Chloride-Secreting Transporter Candidate in Kidney Cyst Epithelium in Tuberos Sclerosis," *Am. J. Pathol.*, vol. 193, no. 2, pp. 191–200, 2023, doi: 10.1016/j.ajpath.2022.10.007.
- [18] C. Ronsin *et al.*, "Incidence, Risk Factors and Outcomes of Kidney and Liver Cyst Infection in Kidney Transplant Recipient With ADPKD," *Kidney Int. Reports*, vol. 7, no. 4, pp. 867–875, 2022, doi: 10.1016/j.ekir.2022.01.1062.
- [19] T. Blanc *et al.*, "Three-dimensional architecture of nephrons in the normal and cystic kidney," *Kidney Int.*, vol. 99, no. 3, pp. 632–645, 2021, doi: 10.1016/j.kint.2020.09.032.
- [20] C. Hanna *et al.*, "High Prevalence of Kidney Cysts in Patients With CYP24A1 Deficiency," *Kidney Int. Reports*, vol. 6, no. 7, pp. 1895–1903, 2021, doi: 10.1016/j.ekir.2021.04.030.
- [21] L. Zhu, Z. Xu, and T. Fang, "Analysis of Cardiac Ultrasound Images of Critically Ill Patients Using Deep Learning," *J. Healthc. Eng.*, vol. 2021, 2021, doi: 10.1155/2021/6050433.
- [22] Z. Shen, W. Li, and H. Han, "Deep Learning-Based Wavelet Threshold Function Optimization on Noise Reduction in Ultrasound Images," *Sci. Program.*, vol. 2021, 2021, doi: 10.1155/2021/3471327.
- [23] L. Alhazmi, "Classification of Ultrasound Images with Convolutional Neural Networks in High-Performance Using IoT," *Wirel. Commun. Mob. Comput.*, vol. 2022, 2022, doi: 10.1155/2022/1688076.
- [24] R. Du, Y. Chen, T. Li, L. Shi, Z. Fei, and Y. Li, "Discrimination of Breast Cancer Based on Ultrasound Images and Convolutional Neural Network," *J. Oncol.*, vol. 2022, 2022, doi: 10.1155/2022/7733583.
- [25] U. Raghavendra *et al.*, "Automated Diagnosis and Assessment of Cardiac Structural Alteration in Hypertension Ultrasound Images," *Contrast Media Mol. Imaging*, vol. 2022, pp. 25–30, 2022, doi: 10.1155/2022/5616939.

- [26] M. Guo *et al.*, “Recognition of Thyroid Ultrasound Standard Plane Images Based on Residual Network,” *Comput. Intell. Neurosci.*, vol. 2021, 2021, doi: 10.1155/2021/5598001.
- [27] Y. Xie, S. Chen, D. Jia, B. Li, Y. Zheng, and X. Yu, “Artificial Intelligence-Based Feature Analysis of Ultrasound Images of Liver Fibrosis,” *Comput. Intell. Neurosci.*, vol. 2022, 2022, doi: 10.1155/2022/2859987.
- [28] K. Ejaz, M. Arif, M. S. M. Rahim, D. Izdrui, D. M. Craciun, and O. Geman, “Confidence Region Identification and Contour Detection in MRI Image,” *Comput. Intell. Neurosci.*, vol. 2022, 2022, doi: 10.1155/2022/5898479.
- [29] S. Mustafa *et al.*, “Entropy and Gaussian Filter-Based Adaptive Active Contour for Segmentation of Skin Lesions,” *Comput. Intell. Neurosci.*, vol. 2022, 2022, doi: 10.1155/2022/4348235.
- [30] F. G. Zollner *et al.*, “Kidney Segmentation in Renal Magnetic Resonance Imaging - Current Status and Prospects,” *IEEE Access*, vol. 9, pp. 71577–71605, 2021, doi: 10.1109/ACCESS.2021.3078430.
- [31] C. Keatmanee, U. Chaumrattanakul, K. Kotani, and S. S. Makhanov, “Initialization of active contours for segmentation of breast cancer via fusion of ultrasound, Doppler, and elasticity images,” *Ultrasonics*, vol. 94, pp. 438–453, 2019, doi: 10.1016/j.ultras.2017.12.008.
- [32] W. J. Zabel *et al.*, “Clinical Evaluation of Deep Learning and Atlas-Based Auto-Contouring of Bladder and Rectum for Prostate Radiation Therapy,” *Pract. Radiat. Oncol.*, vol. 11, no. 1, pp. e80–e89, 2021, doi: 10.1016/j.prro.2020.05.013.
- [33] S. Elmi and Z. Elmi, “A robust edge detection technique based on Matching Pursuit algorithm for natural and medical images,” *Biomed. Eng. Adv.*, vol. 4, no. September, p. 100052, 2022, doi: 10.1016/j.bea.2022.100052.
- [34] R. Rajan and S. Kumar, “Gauss Gradient Algorithm for Edge Detection in Retinal Optical Coherence Tomography Images,” *Procedia Comput. Sci.*, vol. 218, pp. 1014–1026, 2023, doi: 10.1016/j.procs.2023.01.081.
- [35] M. Huang, Y. Liu, and Y. Yang, “Edge detection of ore and rock on the surface of explosion pile based on improved Canny operator,” *Alexandria Eng. J.*, vol. 61, no. 12, pp. 10769–10777, 2022, doi: 10.1016/j.aej.2022.04.019.
- [36] N. Ohs *et al.*, “Automated segmentation of fractured distal radii by 3D geodesic active contouring of in vivo HR-pQCT images,” *Bone*, vol. 147, no. February, p. 115930, 2021, doi: 10.1016/j.bone.2021.115930.
- [37] D. E. Rodriguez-Obregon *et al.*, “Semi-supervised COVID-19 volumetric pulmonary lesion estimation on CT images using probabilistic active contour and CNN segmentation,” *Biomed. Signal Process. Control*, vol. 85, no. March, 2023, doi: 10.1016/j.bspc.2023.104905.
- [38] C. Paz, A. Cabarcos, J. Vence, and C. Gil, “Development of an active contour based algorithm to perform the segmentation of soot agglomerates in uneven illumination TEM imaging,” *Powder Technol.*, vol. 400, 2022, doi: 10.1016/j.powtec.2022.117260.
- [39] A. Cabarcos, C. Paz, R. Pérez-Orozco, and J. Vence, “An image-processing algorithm for morphological characterisation of soot agglomerates from TEM micrographs: Development and functional description,” *Powder Technol.*, vol. 401, 2022, doi: 10.1016/j.powtec.2022.117275.
- [40] W. Liu, L. Wang, and M. Cui, “Quantum Image Segmentation Based on Grayscale Morphology,” *IEEE Trans. Quantum Eng.*, vol. 3, no. June, pp. 1–12, 2022, doi: 10.1109/TQE.2022.3223368.
- [41] Prof. Deepanita Mondal. (2018). Analysis and Evaluation of MAC Operators for Fast Fourier Transformation. *International Journal of New Practices in Management and Engineering*, 7(01), 01 - 07. <https://doi.org/10.17762/ijnpme.v7i01.62>
- [42] Bommi, K. ., & Evanjaline, D. J. . (2023). Timestamp Feature Variation based Weather Prediction Using Multi-Perception Neural Classification for Successive Crop Recommendation in Big Data Analysis. *International Journal on Recent and Innovation Trends in Computing and Communication*, 11(2s), 68–76. <https://doi.org/10.17762/ijritcc.v11i2s.6030>
- [43] Rohokale, M. S., Dhabliya, D., Sathish, T., Vijayan, V., & Senthilkumar, N. (2021). A novel two-step co-precipitation approach of CuS/NiMn2O4 heterostructured nanocatalyst for enhanced visible light driven photocatalytic activity via efficient photo-induced charge separation properties. *Physica B: Condensed Matter*, 610 doi:10.1016/j.physb.2021.412902